

Magnetron Instability in the Low-Space-Charge Limit

Spilios Riyopoulos

Science Applications International Corporation, McLean, Virginia 22102

(Received 7 April 1998)

The resonant interaction between practically stable, smooth cavity diocotron modes and empty-magnetron cavity slow waves generates the unstable “loaded” magnetron cavity modes. In the low-space-charge, guiding center fluid picture, the most unstable frequency nearly satisfies the Buneman-Hartree resonance with the cathode flow surface, and the growth is symmetric around resonance. A negative density gradient, $dn/dr < 0$, is necessary for instability. Because the unstable frequencies scale as the diocotron frequency, $\omega \propto \omega_D$, the relative growth rate, scaling as ω_D/ω , is independent of, and does not go to zero with, $\omega_e^2/\Omega^2 = \omega_D/\Omega = 0$, as it does for diocotron modes. [S0031-9007(98)07160-9]

PACS numbers: 84.40.Fe, 52.20.Dq, 52.40.Hf, 52.80.Pi

The onset of unstable oscillations in periodically structured magnetron cavities has yet to be analytically described, though magnetrons [1] are the earliest sources of microwave devices. Thus far analysis has focused on the stability of non-neutral $\mathbf{E} \times \mathbf{B}$ drifting flows inside smooth wall cavities [2–4]. Short wavelength, slow phase velocity space charge perturbations (diocotron modes) have been shown to be practically stable [2] when the flow touches the cathode (cathode layer). In addition these modes can exist only at frequencies above the cyclotron frequency [3], while spontaneous onset of magnetron oscillations is observed [5] well below cyclotron frequency. It is shown in this Letter that in magnetron cavities, which support slow waves in vacuum, a new instability results from the interaction of the cathode layer with the cavity slow wave; the unstable frequencies are centered around the intersection between the smooth cavity diocotron, and the magnetron cavity slow wave dispersion relations. Recent treatment [6] of a similar situation employed a single harmonic “planarized anode” approximation, leading to a different dispersion relation which did not expose the physics of the diocotron-slow wave coupling and the analytic parameter dependence of the instability.

While smooth cavities support monochromatic slow waves $\omega/ck \ll 1$ only in the presence of a cathode charge layer, magnetron cavities support slow waves in vacuum. Owing to the vane periodicity, a single frequency magnetron mode involves many azimuthal “free space” spatial harmonics of the vane period. It is shown that, when a cathode layer is introduced, a single frequency “loaded” magnetron eigenmode involves a superposition of diocotron-type modes at spatial harmonics of the vane period. The interaction of one, resonant, diocotron harmonic with the vacuum cavity phase velocity generates the instability responsible for the onset of magnetron oscillations. Since the excited frequencies are near the diocotron frequency ω_D , the relative growth rate, scaling as $\omega_D/\omega \sim 1$, is nontrivial in the low space charge limit $\omega_D/\Omega = \omega_e^2/\Omega^2 \ll 1$, where $\omega_e^2 = 4\pi e^2 n_0/m_e$, $\Omega =$

$eB_0/m_e c$ are the plasma and cyclotron frequencies. Unstable magnetron frequencies extend well below the cyclotron Ω , as observed in experiments.

A schematic illustration of the cavity geometry is shown in Fig. 1. A dc voltage V_0 applied across the radius r , combined with a uniform applied magnetic field B_0 in the axial direction z , induces an azimuthal $\mathbf{E} \times \mathbf{B}$ drift flow around the cathode. For a cold fluid (zero Larmor radius) of constant density n_0 , the equilibrium flow profile $\mathbf{u}_0 = u_0 \hat{\theta}$ for $a \leq r \leq h$ is

$$u_0(r) = \frac{eE_0(r)}{m\Omega} = \frac{\omega_e^2}{\Omega^2} \left(r - \frac{a^2}{r} \right), \quad (1)$$

where $E_0(r)$ is the radial field. The space charge limit $E_0(a) = 0$, no slip $u_0(a) = 0$ condition, is imposed at the cathode. For magnetic insulation, $h < b$, V_0 must not exceed the Hull voltage $-eV_H \equiv (1/8)m\Omega^2(b - a^2/b)^2$. We will focus on the low space charge limit $\omega_e^2/\Omega^2 \ll 1$, the density n_0 being much smaller than the Brillouin density n_B such that $\omega_e^2(n_B) = \Omega^2$.

The relevant frequencies are the wave frequency ω , the cyclotron frequency Ω , the plasma frequency ω_e , and the diocotron frequency $\omega_D \equiv \omega_e^2/\Omega$ characterizing the shear in the drift velocity du_0/dr . Since by definition $\omega_D < \omega_e < \Omega$ (ω_e being the geometrical mean of Ω and ω_D), separation of time scales occurs naturally in low space charge situations $\omega_e/\Omega \ll 1$ when dealing with low frequency modes $\omega \propto \omega_D \leq \omega_e$. The ratio ω_D/ω , on the other hand, remains finite with decreasing density by exciting lower cavity frequencies; it will be shown that $\omega_D/\omega \sim 1/n$, n being the azimuthal mode number. Thus, the slow wave, low space charge scaling is adopted, neglecting terms $\omega_e^2/\Omega^2 \sim \omega^2/c^2 k^2 \sim \epsilon^2$ while retaining $\omega/ck \sim \epsilon$ and $\omega_D/\omega \sim \epsilon^0$. That amounts to averaging out the fast cyclotron scale, leaving the drift equations of the guiding center (GC) motion. Accordingly, and for step function density profile $d\omega_e^2/dr = -\omega_e^2 \delta(r - h)$, the full cold fluid description

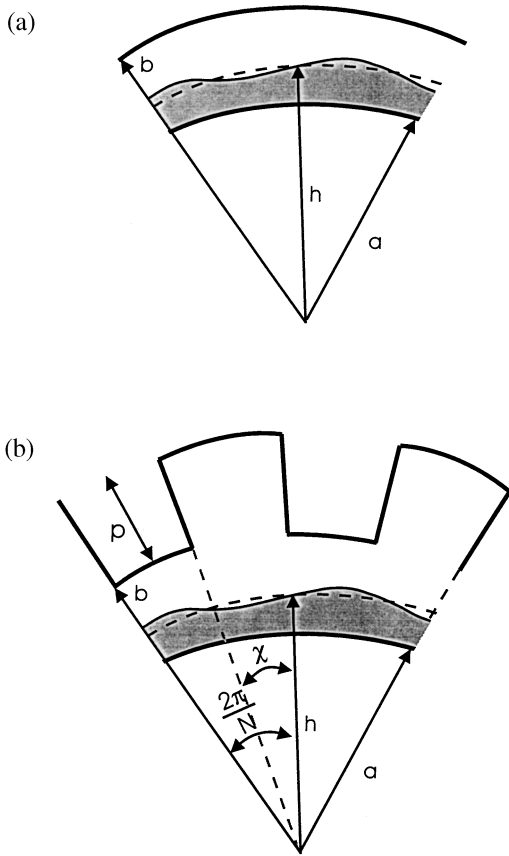


FIG. 1. Geometry illustration of cathode layer flow inside (a) a smooth cylindrical cavity, and (b) a magnetron cavity with periodic anode vanes.

[4] is reduced to the diocotron eigenmode equation [2]

$$\frac{1}{r} \frac{\partial}{\partial r} \left(r \frac{\partial}{\partial r} \right) \psi_n - \frac{n^2}{r^2} \psi_n = -\frac{n}{r} \frac{\omega_D}{\omega - (n/r)u_0(h)} \delta(r-h) \psi_n, \quad (2)$$

with $\Psi_n(r, \theta) = \psi_n(r) e^{in\theta}$ and $E_{\theta n} = (-1/r) \partial \Psi_n / \partial \theta = -(in/r) \psi_n e^{in\theta}$. The dielectric response of the cathode layer is reduced to the δ -function term in the right-hand side, corresponding to the excitation of a surface perturbation at the hub top $r = h$.

$$\Psi_n(r, \theta) = \sum_{j=-\infty}^{\infty} A_{n_j} a^{n_j} C_n^-(r, a) e^{in_j \theta}, \quad a \leq r \leq b, \quad (8)$$

$$\Psi_n(r, \theta) = F \frac{N\chi}{2\pi} \sum_{j=-\infty}^{\infty} \frac{r}{n_j} \frac{\sin(n_j \chi / 2)}{n_j \chi / 2} \sin \left[\frac{\omega}{c} (b + p - r) \right] e^{in_j \theta}, \quad b \leq r \leq b + p. \quad (9)$$

A single frequency mode ω involves superposition of many azimuthal wave number harmonics $n_j = n + jN$, $j = 0, 1, 2, \dots$. The vacuum magnetron cavity dispersion, given by

$$Z_V(\omega, n) \equiv \frac{\cot[(\omega/c)p]}{(\omega/c)p} - \frac{N\chi}{2\pi} \sum_{j=-\infty}^{\infty} \frac{\sin(n_j \chi / 2)}{n_j \chi / 2} \frac{1}{(n_j/b)} \frac{C_{n_j}^+(b, a)}{C_{n_j}^-(b, a)} = 0, \quad (10)$$

exhibits infinite branches (frequency bands) $\omega = \omega_q(n)$, $q = 1, 2, \dots$. Each band is periodic in azimuthal wave number

Equation (2) has been previously solved for (i) a cathode layer in a smooth anode cavity (no vanes) [2] and (ii) an empty structured anode (magnetron) cavity, $\omega_D = 0$ [1]. For a cathode layer inside a smooth anode cavity, the solutions are monochromatic diocotron modes

$$\Psi_n(r, \theta) = A a^n C_n^-(r, a) e^{in\theta}, \quad a \leq r \leq h, \quad (3)$$

$$\Psi_n(r, \theta) = A a^n \left[C_n^-(r, a) + \frac{\omega_D}{2\hat{\omega}} C_n^-(h, a) C_n^-(r, h) \right] e^{in\theta} \quad h < r \leq b, \quad (4)$$

with the definitions $C_n^{\pm}(x, y) = (x/y)^n \pm (y/x)^n$ and

$$\hat{\omega} \equiv \omega - \frac{1}{2} \omega_D \left(1 - \frac{a^2}{h^2} \right). \quad (5)$$

The smooth anode boundary condition $\psi_n(b) = 0$ yields the diocotron dispersion relation in cylindrical geometry

$$Z_d(\omega, n) \equiv C_n^-(b, a) + \frac{\omega_D}{2\hat{\omega}} [C_n^+(b, a) - C_n^+(ab, h^2)] = 0, \quad (6)$$

from which follow stable modes $\Im \omega = 0$ of real frequency

$$\omega_d(n) = \frac{1}{2} \omega_D \left\{ n \left(1 - \frac{a^2}{h^2} \right) - \frac{[1 - (a/h)^{2n}][1 - (h/b)^{2n}]}{1 - (a/b)^{2n}} \right\}. \quad (7)$$

For large azimuthal wave number $n \gg 1$, $\omega_d = \omega_D n (1 - a^2/h^2)/2$. In the above GC approximation, $s \equiv \omega_e^2/\Omega^2 = 0$, diocotron modes are stable for a flow touching the cathode (cathode layer); for finite s they are weakly unstable [3] and their growth tends rapidly to zero, as $e^{-2/s}$.

The empty-magnetron cavity modes are subject to piecewise constant boundary conditions at the vane tips, $E_{\theta} \propto F e^{i2\pi j/N}$ for $2\pi j - \chi/2 < \theta < 2\pi j + \chi/2$, and $E_{\theta} = 0$ otherwise, where χ is the angle subtended by a slot, $j = 0, 1, \dots, N-1$ and N the number of vanes. The cavity modes are Bloch-type modulated waves,

n , $\omega_q(n) = \omega_q(n + jN)$, hence the fundamental $0 < n < N$ in the first Brillouin zone is used for mode labeling. The easiest excited lowest branch corresponds to slow waves propagating at phase velocity $\omega/(n/r)$ much smaller than c .

The cathode layer dispersion inside a periodically structured anode is now introduced, with the details described elsewhere [7]. The magnetron mode structure below the vane tips $a \leq r \leq b$ is a superposition of diocotron-type solutions (3) and (4) over the vane harmonics $n_j = n + jN$, replacing the free space harmonics in (8). The fields inside the vane gaps retain their vacuum cavity structure of (9). Eliminating coefficients [7], by matching E_θ and

B_z at the vane tips $r = b$, where $\partial B_z/\partial r = (i\omega/c)E_\theta$, yields the following dispersion relation for a cathode layer in a magnetron cavity:

$$Z(\omega, n) \equiv Z_V(\omega, n) - \sum_{j=-\infty}^{\infty} \frac{\omega_D}{2\omega} \frac{\Xi_{n_j}}{Z_d(\omega, n_j)} = 0. \quad (11)$$

In (11), the dispersion of a vacuum magnetron mode is coupled to the dispersions of diocotron modes over all of the vane spatial harmonics $n_j = n + jN$. The coupling strength is proportional to the diocotron frequency ratio ω_D/ω , while $\Xi_{n_j} \equiv \xi_{n_j} C_{n_j}^+(b, a)$ and

$$\xi_{n_j} = -\frac{\sin(n_j\chi/2)}{(n_j\chi/2)} \frac{N\chi/2\pi}{(n_j/b)p} \left\{ \frac{C_{n_j}^-(b, a)}{C_{n_j}^+(b, a)} - \frac{C_{n_j}^+(b, a)[C_{n_j}^+(b, a) - C_{n_j}^+(ab, h^2)]}{[C_{n_j}^-(b, a)]^2} \right\} \quad (12)$$

are purely geometrical factors. It is the interaction between smooth diocotron and structured anode modes that creates unstable magnetron modes.

Although (11) is valid for arbitrary ω_D/ω , the stability properties are easier to analyze in the small $\omega_D/\omega \sim \epsilon$ limit. Then, of all the Ξ_{n_j} terms, only resonant diocotron harmonic(s) $Z_d(\omega, n_l) \approx 0$ make an important contribution. Singling out one resonant term, for $j = l$, and rearranging (11), leads to

$$\left[Z_V(\omega, n) - \frac{\omega_D}{2\omega} Z \right] [\omega - \omega_d(n_l)] - \frac{\omega_D}{2} \xi_{n_l} = 0, \quad (13)$$

where Z contains all of the nonresonant terms $Z = \sum_{j \neq l} \Xi_{n_j}/Z_d(\omega, n_j)$. If ξ_{n_l} is formally set to zero (but ω_D remains finite), the solutions decouple into independently propagating magnetron cavity modes $\omega = \omega_V(n)$, solutions of $Z_V(\omega, n) = 0$, and smooth anode diocotron modes $\omega = \omega_d(n_l)$, solutions of $Z_d(\omega, n_l) = 0$, depicted in Fig. 2. For finite $\omega_D \xi_{n_l}$ an instability arises around the intersection of the empty cavity and the diocotron mode branches $\omega_d(n_l) \approx \omega_V(n)$. For small $\omega_D/\omega \approx \epsilon$ the dispersion $Z_V(\omega, n)$ can be expanded about ω_d , $Z_V = Z_0 + Z_0'(\omega - \omega_d)$, where $Z_0 \equiv Z_V(\omega_d)$ and Z_0' obtained from (10). Substituting in (13) and solving the resulting quadratic equation yields the loaded cavity magnetron mode dispersion

$$\omega = \omega_d(n_l) + \frac{-(Z_0 - Z) \pm \sqrt{(Z_0 - Z)^2 + 2\omega_D \xi_{n_l} Z_0'}}{2Z_0'}, \quad (14)$$

valid for small ω_D/ω [the numerical solution of (13) must be used for $\omega_D/\omega \leq 1$]. Complex roots (instability) occur in the frequency range where

$$0 < (Z_0 - Z)^2 < -2\omega_D \xi_{n_l} Z_0'. \quad (15)$$

Figure 3 plots the growth rate near the π mode $n = 8$ in a 16 vane cavity with $\chi = \pi/16$ for $\omega_D/\omega_\pi = 0.60$ and the following cavity parameters (normalized

to ω/c): $a = 0.0908$, $b = 0.182$, $h = 0.134$, and $p = 1.24$. Given that Z_0' in Eq. (15) is generally negative, the right-hand side inequality is satisfied for $\xi_l > 0$, obtained for a negative density step $dn_0/dr < 0$.

Although a given cavity frequency $\omega(n)$ may resonate with a diocotron mode through any one of the vane harmonics $n_l = n + lN$, maximum magnetron growth occurs at the fundamental resonance ($l = 0$), $\omega(n) = \omega_d(n)$, as Ξ_{n_l} diminishes rapidly with l . The most unstable frequency is such that the empty cavity angular phase velocity $(1/r)\omega/(n/r) = \omega/n$ nearly matches the angular flow velocity at the hub top h ; from Eq. (7)

$$\frac{\omega}{n} \approx \frac{1}{2} \omega_D \left[\left(1 - \frac{a^2}{h^2} \right) - \frac{1}{n} \right], \quad (16)$$

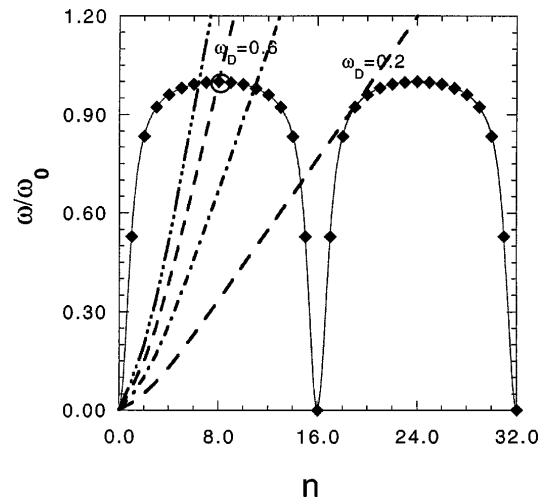


FIG. 2. Intersections of an $N = 16$ vane magnetron cavity vacuum dispersion (light solid line), with smooth diocotron mode dispersion curves (broken lines) of various diocotron frequencies ω_D and drift velocities $u_0(h)$. Diamonds mark magnetron cavity modes of integer n , and frequency is normalized to the empty cavity π -mode frequency, $\omega_V(N/2) = 1$. Strong magnetron-diocotron coupling occurs at the intersections $\omega_V(n) = \omega_d(n_j)$.

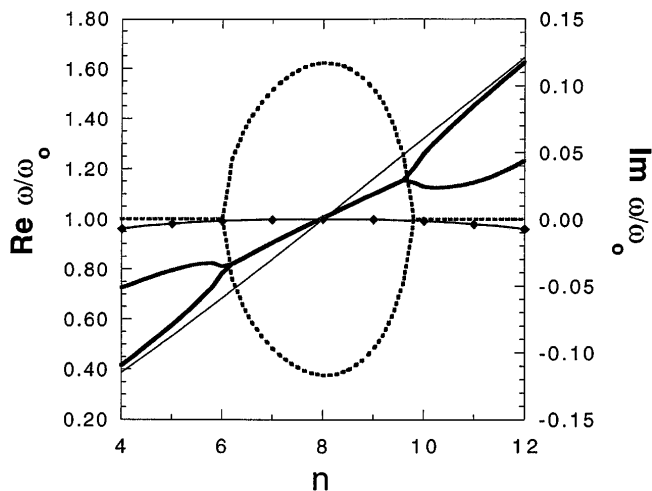


FIG. 3. Magnetron instability for magnetron-diocotron resonance at the π mode $n = 8$ (marked by circle in Fig. 2). The real frequencies of the two “loaded cavity” branches (solid lines) are shown against the (uncoupled) magnetron and diocotron branches (light solid) of Fig. 2. Heavy dashed lines mark the loaded cavity imaginary frequencies (growth rates). The modes $n = 7$ and $n = 9$ are also unstable.

valid at large n . Thus, the exact frequency falls below the Buneman-Hartree (BH) resonance at the hub top $\omega_{\text{BH}} = (1/2)\omega_D(1 - a^2/h^2)$, and corresponds to a resonance below the surface; it asymptotes to the surface at $n \gg 1$. The maximum growth rate

$$\gamma_0 \approx \omega_D \sqrt{\frac{(\xi_0/2)(1 - a^2/h^2) \sin^2[(\omega_d/c)p]}{1 + \cot[(\omega_d/c)p]/(\omega_d/c)p}} \quad (17)$$

is roughly proportional to, but not quite linear in, the diocotron frequency $\omega_D = \omega_e^2/\Omega$, as the quantity inside the root has a weak dependence on ω_D . There is a finite width of unstable frequencies around the BH resonance, given implicitly by (15). The growth rates are nearly *symmetric* around the resonant frequency ω_d , confirming earlier results in the small signal (i.e., nonexponential growth) crossed-field amplifier gain analysis [8]. Gain symmetry distinguishes crossed field from the rest of the microwave devices, which exhibit *antisymmetric* growth rates with zero at exact resonance. Combining (16) and (17) shows that the relative maximum growth $\gamma_0/\omega(n)$ increases with decreasing mode number n . Earlier treatment [6] did not reach the above conclusions, nor the diocotron-slow wave coupling dispersion (11).

The maximum growth rate from (17) at the π mode $n = N/2$ is plotted in Fig. 4 versus the charge density parametrized by ω_D ; the surface radius h is adjusted from (16) so that the resonant frequency corresponds to π -mode resonance. Various curves correspond to different number of cavity vanes N , by adjusting the slot angle $\chi = 2\pi/N$ (Fig. 1), for the same dimensions. The growth rate increases nearly proportional to ω_D . For large $\omega_D/\omega \sim 1$ the analytic growth in Fig. 4 exceeds the exact value, from the numerical solution of (13), by 20%.

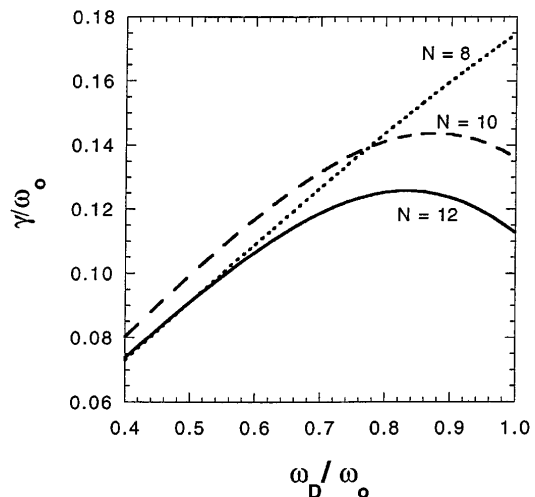


FIG. 4. Maximum π -mode growth rate $n = N/2$ vs diocotron frequency ω_D , in cavities with different vane numbers N . The π -mode frequency is always normalized to 1.

In conclusion, the loaded cavity, low-space-charge magnetron dispersion involves the coupling among the dispersions of practically stable smooth anode diocotron modes and empty-magnetron cavity modes. Strongly unstable magnetron modes arise at the intersections among the above dispersion branches. In the GC approximation the growth rate scales as $\gamma/\omega \sim \omega_D/\omega \sim (1/n)(1 - a^2/h^2)^{-1}$ and is independent of $\omega_e^2/\Omega^2 = 0$. A negative density gradient is required for instability, contrasting an opposite conclusion for smooth cavities [4].

Although the low space charge results are not directly applicable to magnetrons operating at high space charge, extrapolations to $\omega_e^2/\Omega^2 \approx 1$ yield the correct order of magnitude for the instability growth times. The growth rate dependence on various parameters agrees qualitatively with detailed experimental observations of spontaneous growth [5]; strong, $\propto \omega_D$ growth rate peaks near the BH resonance, the growth rate increases with decreasing mode number n , the growth rate increases with charge density (which, in the Brillouin limit scales as the magnetic field $\omega_e \approx \Omega$), and instability (startup) occurs well below the cyclotron frequency.

The author is indebted to B. Vyse for his motivation.

- [1] G. B. Collins, in *Microwave Magnetrons*, edited by G. B. Collins (McGraw-Hill, New York, 1948), pp. 1–42; N. Kroll *ibid*, pp. 49–77.
- [2] R. H. Levy, *Phys. Fluids* **8**, 1288 (1965).
- [3] O. Buneman, R. H. Levy, and L. M. Linson, *J. Appl. Phys.* **37**, 3203 (1966).
- [4] R. C. Davidson, K. T. Tsang, and J. A. Swegle, *Phys. Fluids* **27**, 2332 (1984).
- [5] B. Vyse, Ph.D. thesis, University of Edinburgh, 1971.
- [6] V. M. Ayers, H. C. Chen, R. A. Stark, H. S. Uhm, and H. E. Brandt, *Phys. Fluids B* **4**, 3396 (1992).
- [7] S. Riyopoulos, *Phys. Plasmas* (to be published).
- [8] S. Riyopoulos, *IEEE J. Quantum Electron.* **31**, 1579 (1995).